Supplemental material to

Assessing the spatial and temporal variability of MeHg biogeochemistry and bioaccumulation in the Mediterranean Sea with a coupled 3D model

Ginevra Rosati[1], Donata Canu[1], Paolo Lazzari[1], Cosimo Solidoro[1]

[1] *National Institute of Oceanography and Applied Geophysics – OGS*

Content:

Table S1. Partition coefficients used in the modeling (Choe et al., 2003; Choe and Gill, 2003; Lamborg et al., 2016).

$K_{D\ Hg\text{-}POC}$	*Partition coefficient for HgII and POC*	$l\ kg^{-1}$	$1 \cdot 10^6$
$K_{D\ MMHg\text{-}POC}$	*Partition coefficient for MMHg and POC*	$l\ kg^{-1}$	$5 \cdot 10^5$
$K_{D\ Hg\text{-}DOC} =$	*Partition coefficient for HgII and DOC*	$l\ kg^{-1}$	$2 \cdot 10^5$
$K_{D\ MMHg\text{-}DOC}$	*Partition coefficient for MMHg and DOC*	$l\ kg^{-1}$	$5 \cdot 10^5$

Table S2. Equations S1-S9, used in the model for the calculation of rate for Hg transformations (Zhang et al., 2020, Zhang et al., 2014).

Parameter		Units	Formula		Ref
$\boldsymbol{k_{met}}$	*Hg^{II} methylation rate constant*	d^{-1}	$k_{met} = x_{met} \cdot remPOC$	*Eq. S1*	*1*
	MMHg methylation rate constant	d^{-1}	$k_{met2} = x_{met2}$	*Eq. S2*	*1*
$\boldsymbol{k_{phdm}}$	*MMHg photo-demethylation rate constant*	d^{-1}	$k_{phdm} = x_{phdm} \cdot h\upsilon$	*Eq. S3*	*1*
$\boldsymbol{k_{phdm2}}$	*DMHg photo-demethylation rate constant*	d^{-1}	$k_{phdm2} = x_{phdm2} + 3 \cdot 10^{-4} \cdot h\upsilon$	*Eq. S4*	*1*
$\boldsymbol{k_{dem}}$	*MMHg dark demethylation rate constant*	d^{-1}	$k_{dem} = 9.5 \cdot 10^{-4} + exp(-5500\ \cdot (\frac{1}{T} - \frac{1}{293.15}))$	*Eq. S5*	*1*
$\boldsymbol{k_{phox}}$	*Hg^0 photoxidation rate constant*	d^{-1}	$k_{phox} = x_{phox} \cdot h\upsilon$	*Eq. S6*	*2*
$\boldsymbol{k_{phr}}$	*Hg^{II} photoreduction rate constant*	d^{-1}	$k_{phr} = x_{phr} \cdot h\upsilon$	*Eq. S7*	*2*
$\boldsymbol{k_{biox}}$	*Hg^0 biotic oxidation rate constant*	d^{-1}	$k_{biox} = 0.138 \cdot remPOC$	*Eq. S8*	*2*
$\boldsymbol{k_{biored}}$	*Hg^{II} biotic reduction rate constant*	d^{-1}	$k_{bred} = 0.086 \cdot remPOC$	*Eq. S9*	*2*
$\boldsymbol{x_{met}}$	*Coefficient for Hg methylation*	$m^3\ mmol^{-1}$	0.038		*1*
$\boldsymbol{x_{met2}}$	*Coefficient for MMHg methylation*	d^{-1}	0.0008		*1*
$\boldsymbol{x_{phdm}}$	*Coefficient for MMHg photo-demethylation*	$m^2\ W^{-1}\ d^{-1}$	0.007		*1*
$\boldsymbol{x_{phdm2}}$	*Coefficient for DMHg photo-demethylation*	$m^2\ W^{-1}\ d^{-1}$	0.02		*1*
$\boldsymbol{x_{phox}}$	*Coefficient for biotic oxidation*	$m^3\ mmol^{-1}$	0.56		*2*
$\boldsymbol{x_{phr}}$	*Coefficient for biotic reduction*	$m^3\ mmol^{-1}$	0.14		*2*
remPOC	*POC remineralization*	$mmol\ m^{-3}\ d^{-1}$	BFM model output		
hυ	*Shortwave radiation flux*	$W\ m^{-2}$	BFM model output		
1. Zhang et al., 2020 2. Zhang et al., 2014					

Table S3. Phytoplankton functional types (pfts) of the BFM model with estimated cell-size parameters (radius, surface area, volume, and R_{SV}).

Pft	Functional group	Radius (μm)	Surface	Volume	R_{SV}
P1	*Diatoms*	55	38,013.24	696,909.38	0.05
P2	*Aut. nanoflagellates*	5.5	380.13	696.91	0.55
P3	*Picoplankton*	0.55	3.80	0.70	5.45
P4	*Large phytoplankton*	150	282,743.10	14,137,155.00	0.02

Table S4. Conversion factors used to convert carbon variables of plankton pfts to Wet Weight, derived from published experimental data (Jørgensen et al., 1979).

	Carbon as % of Dry Weight	Dry Weight /Wet Weight Ratio	Carbon/Wet Weight ratio	Applied to pft
Diatoms	37.5	0.31	8.6002	P1
Cyanobacteria	46.69	0.563	3.0842	P3
Chlorophyceae	42.5	0.4705	5.0009	P2
Dinoflagellata	NA *	0.341	7.8201	P4
Carnivorous mesozooplankton	44	11.6	19.6	Z3-Z6
	** used diatoms conversion factor*			

Table S5. Summary of information used to set initial conditions for Hg species in the Mediterranean Sea (Horvat et al. 2003; Cossa and Coquery 2005; Kotnik et al. 2007, 2015; Cossa et al. 2017).

ALB				**SWM**			
Hg_T	*average profile from figure*	*August 2003*	*1*	**Hg_T**	*average profile from figure*	*August 2003 March/April 2004*	*1, 2*
MeHg	*average profile from figure*	*August 2003*	*1*	**MeHg**	*average profile from figure*	*August 2003 March/April 2004*	*1*
DMHg	*from estimated DMHg:DGM ratio in NWM*	-	*2*	**DMHg**	*from estimated DMHg:DGM ratio in NWM*	-	*2*
DGM	*average profile from figure*	*August 2003*	*1*	**DGM**	*average profile from figure*	*August 2003 March/April 2004*	*1*
Hg^0	*by difference (DGM-DMHg)*	-	-	**Hg^0**	*by difference (DGM-MHg)*	-	-
Hg^{II}	*by difference (HgT-MMHg-DMHg-Hg0)*	-	-	**Hg^{II}**	*by difference (HgT-MMHg-DMHg-Hg0)*	-	-
NWM				**CWM**			

Hg_T	*average profile from figure*	*August 2000 March/April 2004*	*2*	**Hg_T**	*st. 19 profile from table*	*Jul/Aug 2000*	*4*
MeHg	*average profile from figure*	*May 2006*	*3*	**MeHg**	*st. 19 profile from table*	*Jul/Aug 2000*	*4*
DMHg	*average profile from figure*	*August 2000 March/April 2004*	*2*	**DMHg**	*st. 19 profile from table*	*Jul/Aug 2000*	*4*
DGM	*average profile from figure*	*August 2000*	*1*	**DGM**	*st.19 profile from figure*	*Jul/Aug 2000*	*5*
Hg^0	*by difference (DGM-DMHg)*	-	-	**Hg^0**	*by difference (DGM-DMHg)*	-	-
Hg^{II}	*by difference (HgT-MMHg-DMHg-Hg0)*	-	-	**Hg^{II}**	*by difference (HgT-MMHg-DMHg-Hg0)*	-	-
TYR				**SIC**			
Hg_T	*average profile from figure*	*August 2000 March/April 2004*	*1, 2*	**Hg_T**	*average profile from figure*	*March/April 2004*	*1*
MeHg	*average profile from figure*	*August 2003 March/April 2004*	*1*	**MeHg**	*average profile from figure*	*March/April 2004*	*1*
DMHg	*estimated based on DMHg:DGM ratio in NWM*		-	**DMHg**	*estimated based on DMHg:DGM ratio in NWM*		-
DGM	*average profile from figure*	*August 2003 March/April 2004*	*1*	**DGM**	*average profile from figure*	*March/April 2004*	*1*
Hg^0	*by difference (DGM-DMHg)*	-	-	**Hg^0**	*by difference (DGM-DMHg)*	-	-
Hg^{II}	*by difference (HgT-MMHg-DMHg-Hg0)*	-	-	**Hg^{II}**	*by difference (HgT-MMHg-DMHg-Hg0)*	-	-
ION				**LEV**			
Hg_T	*average profile from figure*	*August 2003*	*1*	**Hg_T**	*from ION profile*	*August 2003*	*1*
MeHg	*average profile from figure*	*August 2003*	*1*	**MeHg**	*average profile from figure*	*August 2003*	*1*
DMHg	*estimated based on DMHg:DGM ration in NWM*	-	-	**DMHg**	*estimated based on DMHg:DGM ratios in NWM*	-	-
DGM	*average profile from figure*	*August 2003*	*1*	**DGM**	*average profile from figure*	*August 2003*	*1*
Hg^0	-	-		**Hg_T**	-	-	-
Hg^{II}	-	-		**MeHg**	-	-	-
NAD				**SAD**			
HgT	*average profile from stations in Table S1 and S2*	*October/November 2004 June 2005*	*6*	**DGM**	*average profile from stations in Table S1 and S2*	*October/November 2004 June 2005*	*6*

MMHg	*average profile from Table S1 and S2*	*October/November 2004 June 2005*	*6*	**Hg^0**	*average profile from stations in Table S1 and S2*	*October/November 2004 June 2005*	*6*
DMHg	*average profile from Table S1 and S2*	*October/November 2004 June 2005*	*6*	**Hg^{II}**	*average profile from Table S1 and S2*	*October/November 2004 June 2005*	*6*
DGM	*average profile from Table S1 and S2*	*October/November 2004 June 2005*	*6*	**DGM**	*average profile from Table S1 and S2*	*October/November 2004 June 2005*	*6*
	1. Kotnik et al 2007; 2. Cossa e& Coquery 2005; 3. Cossa et al 2017; 4. Horvat et al 2003; 5. Ferrara e al 2003; 6. Kotnik et al 2015						

Equation S10. Parameterization for Hg methylation tested in model sensitivity analysis as alternative to equation S1.

$$k_{met} = x_{met} \cdot (remPOC + remDOC) \quad \textit{Eq. S10}$$

Text S1. Results of the sensitivity analyses

The sensitiviy analysis highlighted that the sinking velocity of organic detritus (POC) has a strong impact of on the vertical profiles of MeHg (MMHg+DMHg), by controlling the vertical distribution of POC concentrations and, consequently, of POC remineralization rates. The POC sinking velocity also affect the sinking velocity of particulate Hg species (Hg^{II}_P and $MeHg_P$), however the small differences among vertical profiles of Hg^{II} indicate this process has a limited impact, likely due to the small fraction represented by particulate Hg species (<1%-2%) in the open sea, where particle concentrations are low (~0.02 mg/l). The hypothesis of POC sinking velocity influencing the vertical distribution of Hg species was thus confirmed, with a stronger effect on MMHg than on inorgainc Hg (Figure S1).

The hypotesys of an increase in modeled MeHg concentrations at higher sinking velocity, driven by a deepening of the net Hg methylation limiting the photochemical degradation of MeHg was instead disproven, as modeled maxima of MeHg concentrations are ~0.15 pM for all the three sensitivity simulations (Figure S1), which is far from the observed MeHg maxima (>0.4 pM) from various cruises in the Mediterranean Sea (Cossa et al., 2009). These, as well as other (e.g. Cossa et al., 2018; Heimbürger et al., 2010), field observations show that the peaks of MeHg profiles were located between ~250 and ~500 m-depth at most of Mediterranean deep stations, which is best reproduced in simulation *vs10* (Figures S1 and 5), adopting the same sinking speed (10 m/d) used in the global coupled biogeochemical Hg model (Ward et al., 2012; Zhang et al., 2020).

The inclusion of the DOC remineralization in the equation for Hg methylation, led to a MeHg increase only in surface waters (Figure S2), while a threefold increase in the Hg methylation constant x_{met} causes MeHg concentrations increase at the depths where maxima MeHg concentrations have been observed (Cossa et al., 2009). The results analyses in the manuscript focus on simulation with *vs=10 m/d* and increased x_{met}.

Figure S1. Sensitivity to POC sinking velocity (v_s) of modeled profiles of HgII concentrations, MeHg concentrations, and POC remineralization flux and concentrations. The output shown are mediated for August 2017 for the subbasins SAD (upper panels), NWM (central panels), and LEV (bottom panels). Blue lines indicate the output of simulation vs3 (POC sink = 3 m/d), green lines indicate the output of simulation vs10 (POC sink = 10 m/d), and yellow lines indicate the output of simulation vs20 (POC sink = 20 m/d).

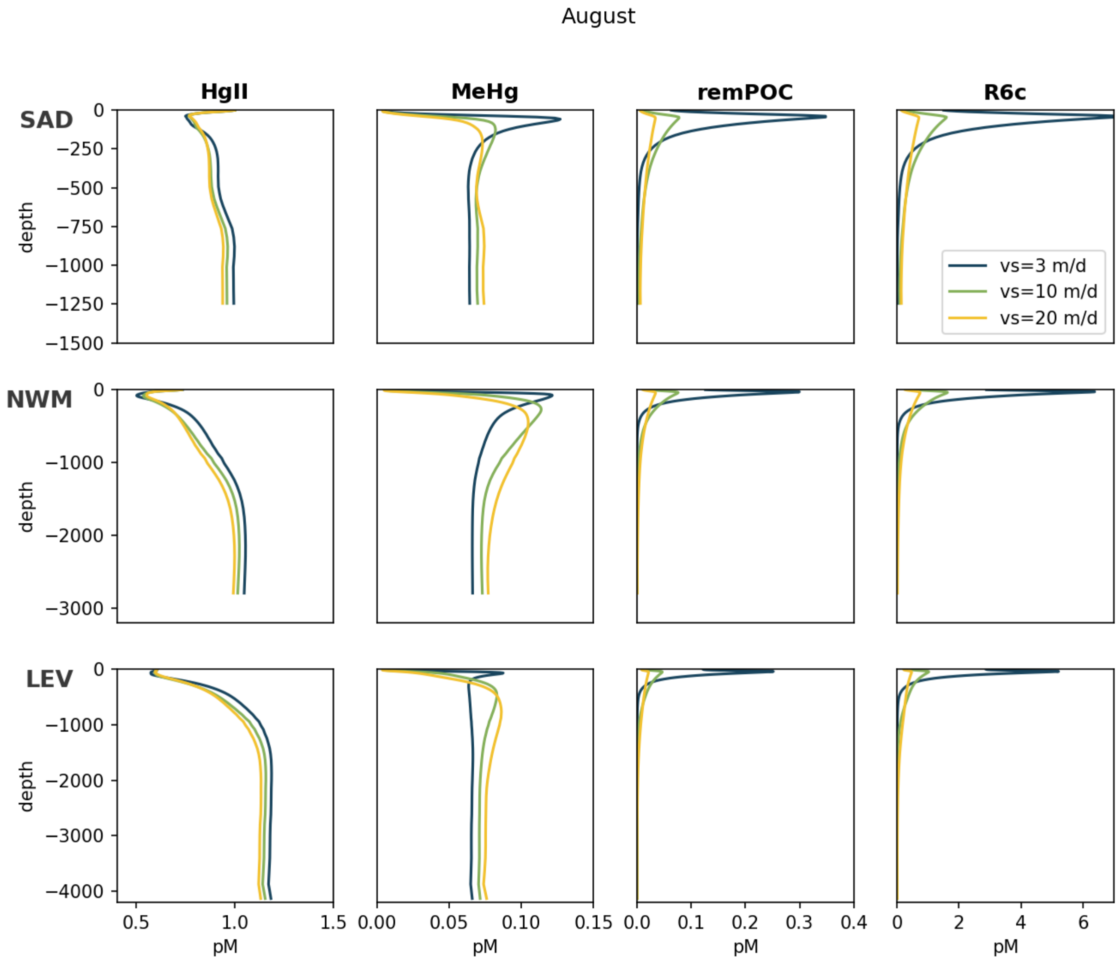

Figure S2. Sensitivity of modeled MeHg concentrations to different parameterization of Hg methylation. The output shown are mediated for May, June, July, and August 2017 for the subbasins SAD (upper panels), NWM (central panels), and LEV (bottom panels). Green lines indicate the output of the base simulation with the parameterization given in Table S1, blue lines indicate the parameterization that include both POC and DOC remineralization, and yellow lines indicate the output of simulation with the threefold increase of Hg methylation constant x_{met}.

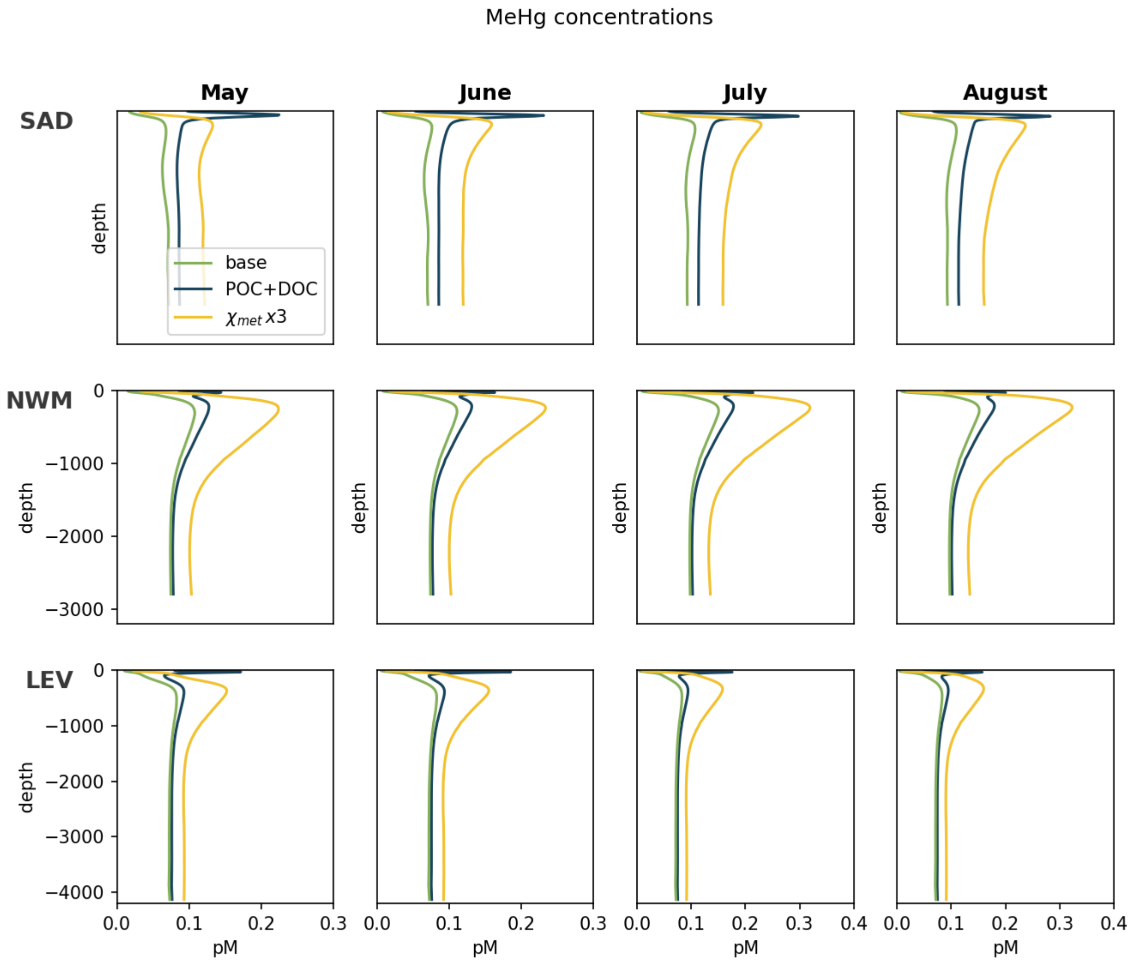

Figure S3. Comparison between monthly averaged modeled HgT concentrations profiles for 2017, after 13 years of model spin-up, and experimental observations from the literature that were used to constrain model initial conditions (Table S5). The observations are from Cossa et al., (2009) (*) and Kotnik et al., (2015) (^).

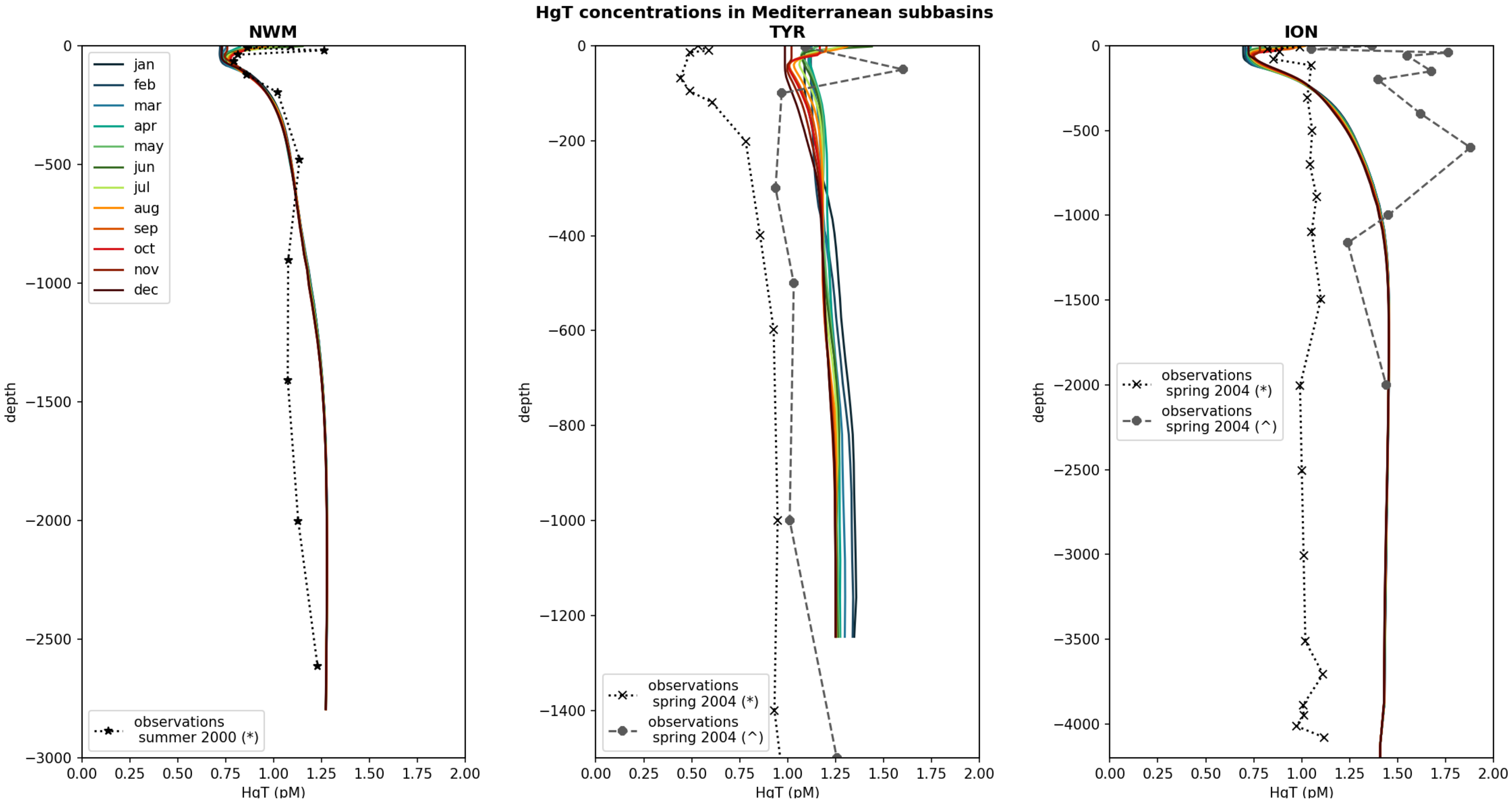

Figure S4. Monthly evolution of modeled reactions rate constants (1/d) for photodemethylation (k_{phdm}), dark demethylation (k_{dem}), and Hg methylation (k_{met}) for each subbasin (colored markers) of the Mediterranean Sea (black lines), depth-integrated for surface water (0-100 m depth), intermediate water (100-600 m depth), and deep water (>600 m depth). The rate constants are computed by the model depending on environmental conditions (Table S2).

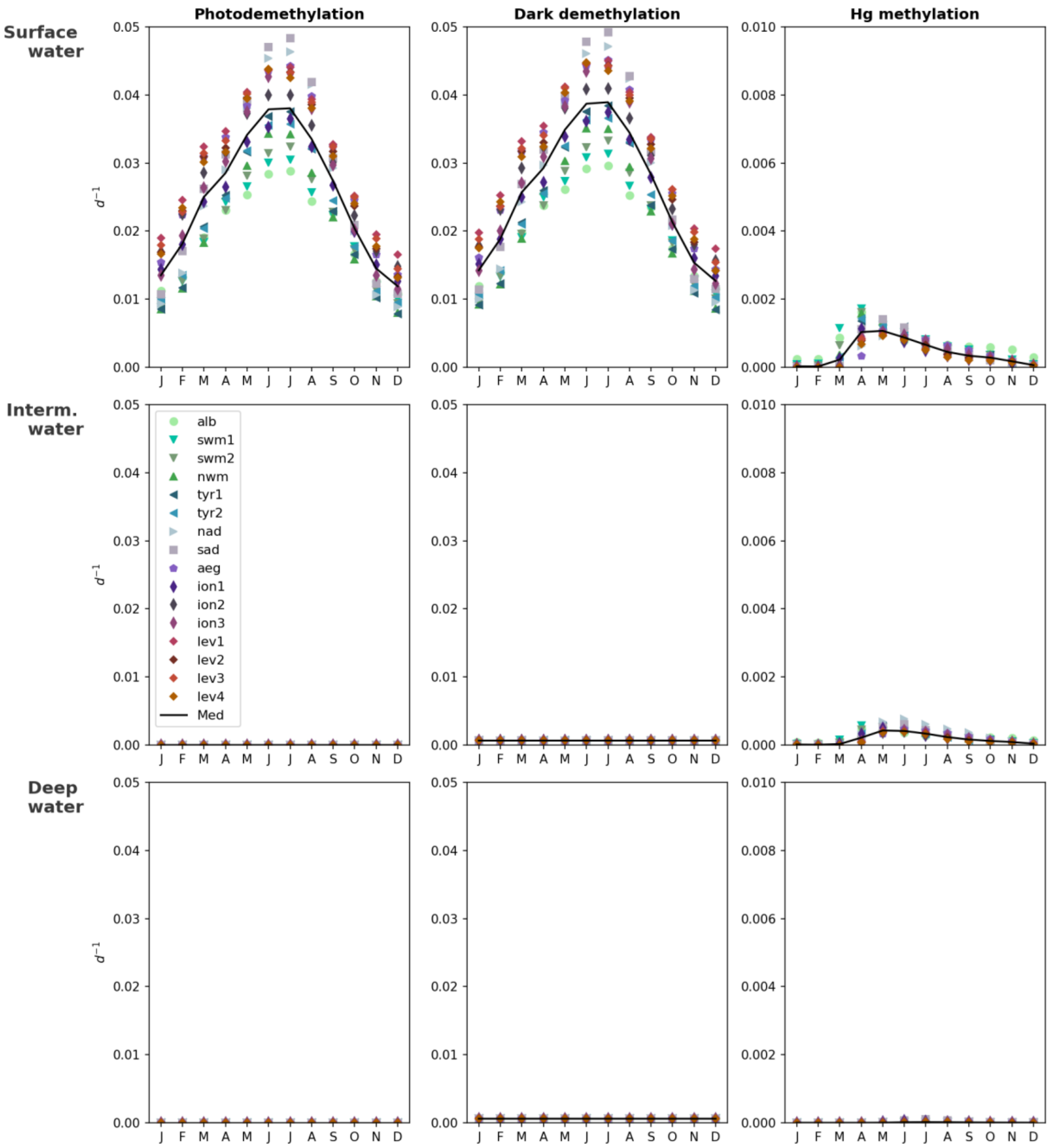

Figure S5. Spatial-temporal distribution of picophytoplankton biomasses on a carbon basis ($C_{phy,\,P3}$).

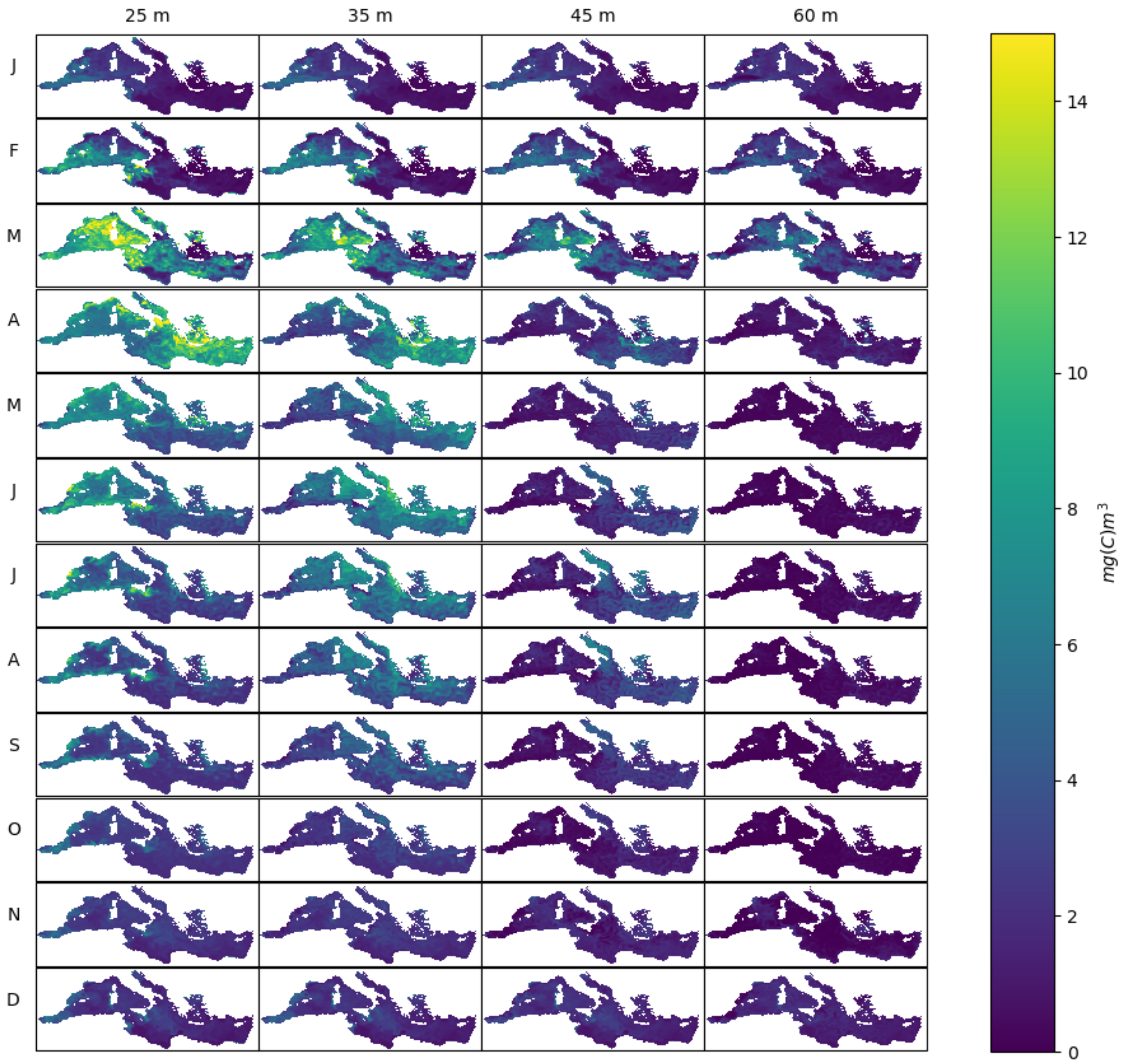

Figure S6. Spatial-temporal distribution of monomethylmercury (MMHg) concentrations in the surface water of the Mediterranean Sea.

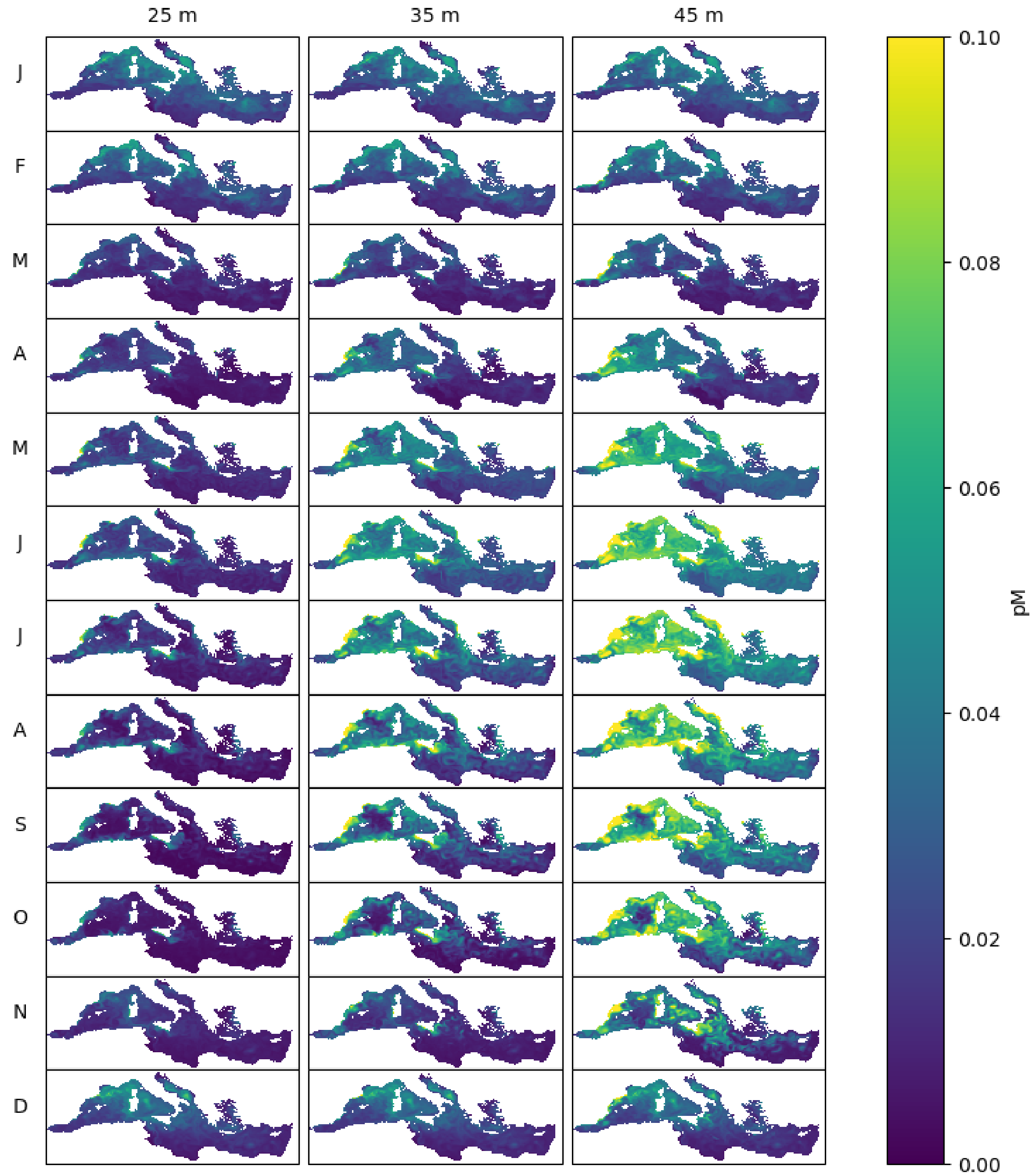

Figure S7. Spatial-temporal distribution of MMHg in picophytoplankton ($MMHg_{phy, P3}$).

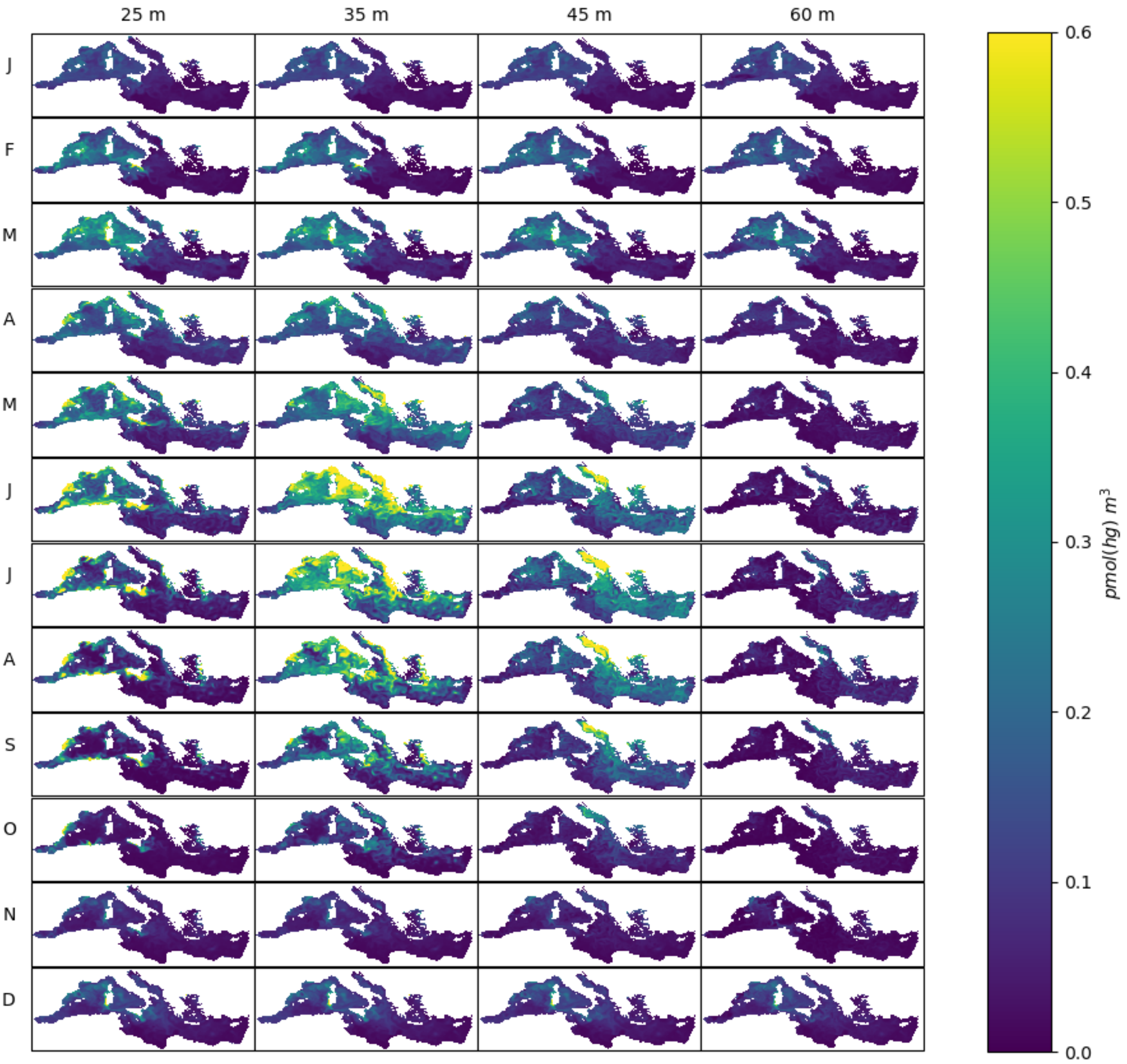

Figure S8. Spatial-temporal distribution of MMHg in autotrophic nanoflagellates ($MMHg_{phy,\,P2}$).

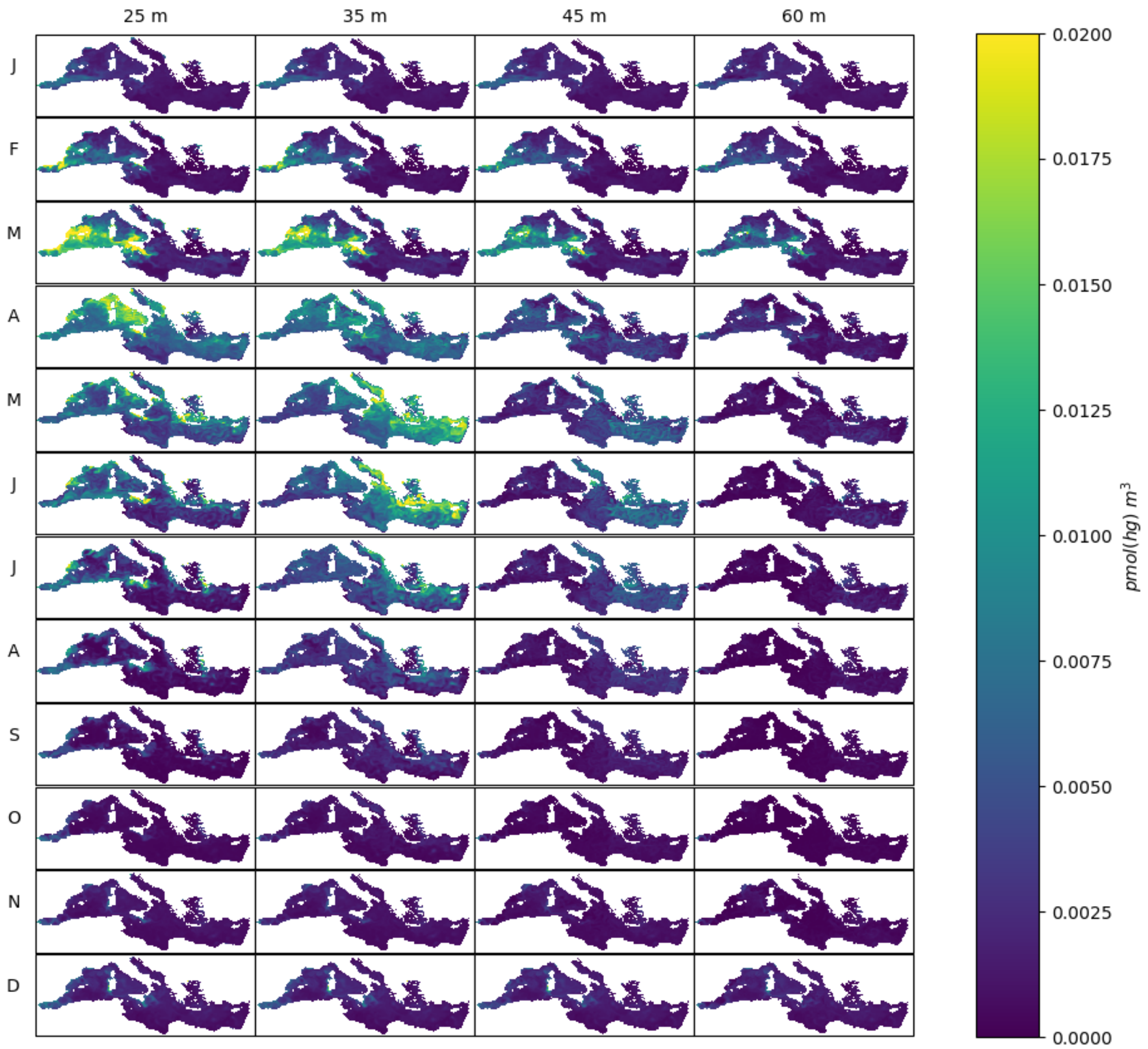

Figure S9. Spatial-temporal distribution of MMHg in diatoms ($MMHg_{phy,P1}$).

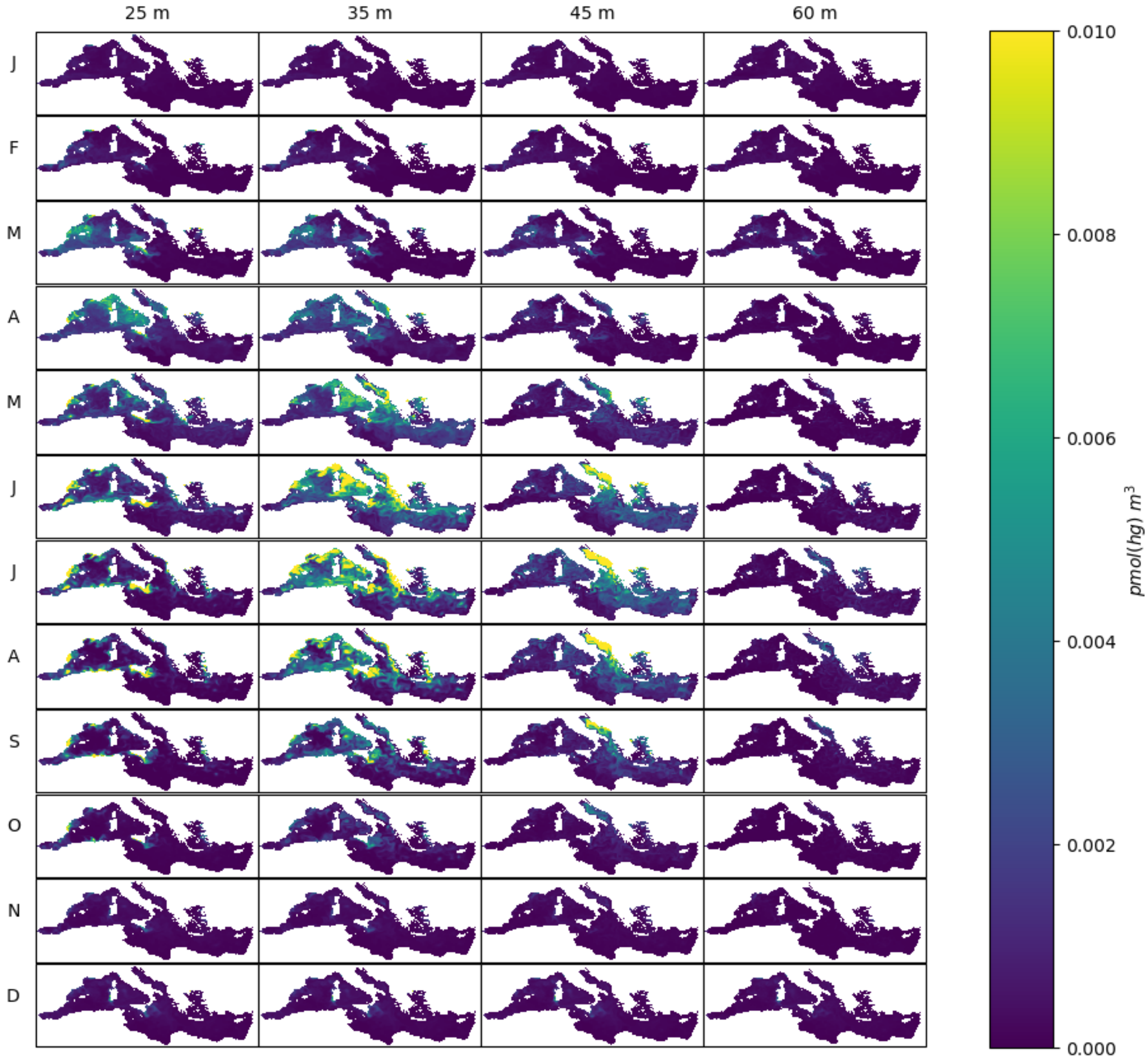

Figure S10. Spatial-temporal distribution of MMHg in large plankton ($MMHg_{phy,\ P4}$).

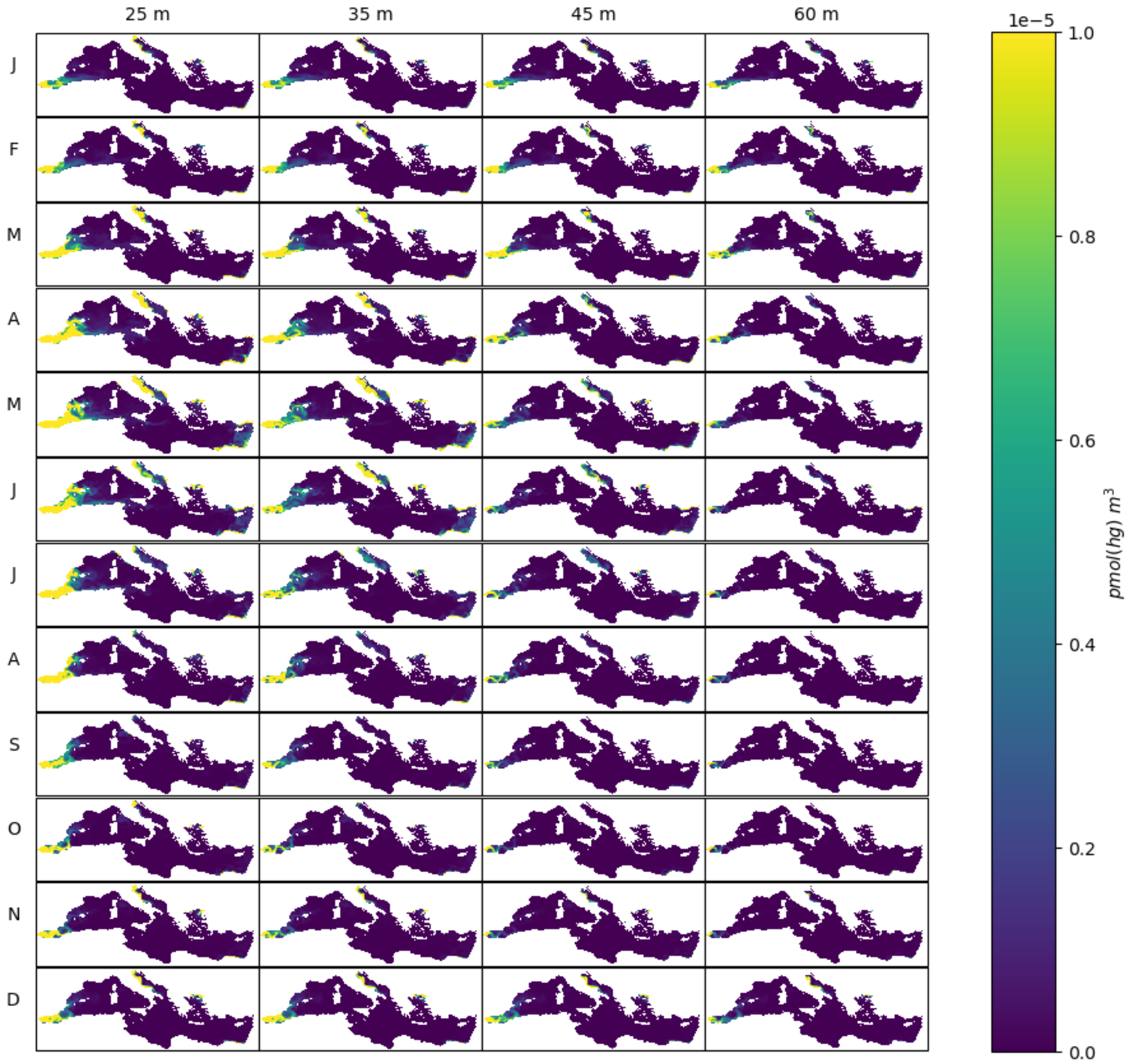

Figure S11. Spatial-temporal distribution of MMHg in heterotrophic nanoflagellates ($MMHg_{zoo,\,Z6}$).

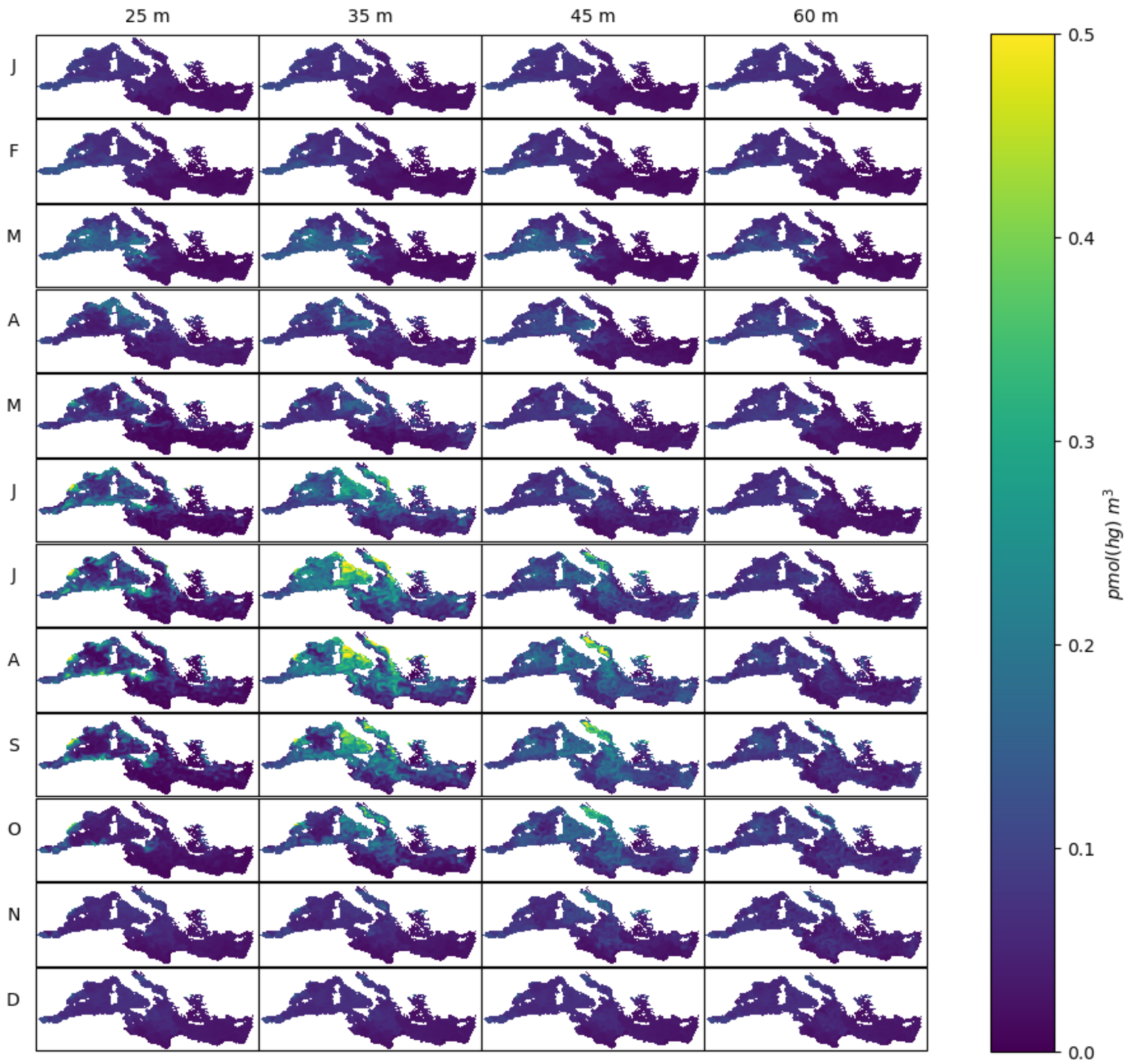

Figure S12. Spatial-temporal distribution of MMHg in microzooplankton ($MMHg_{zoo,Z5}$).

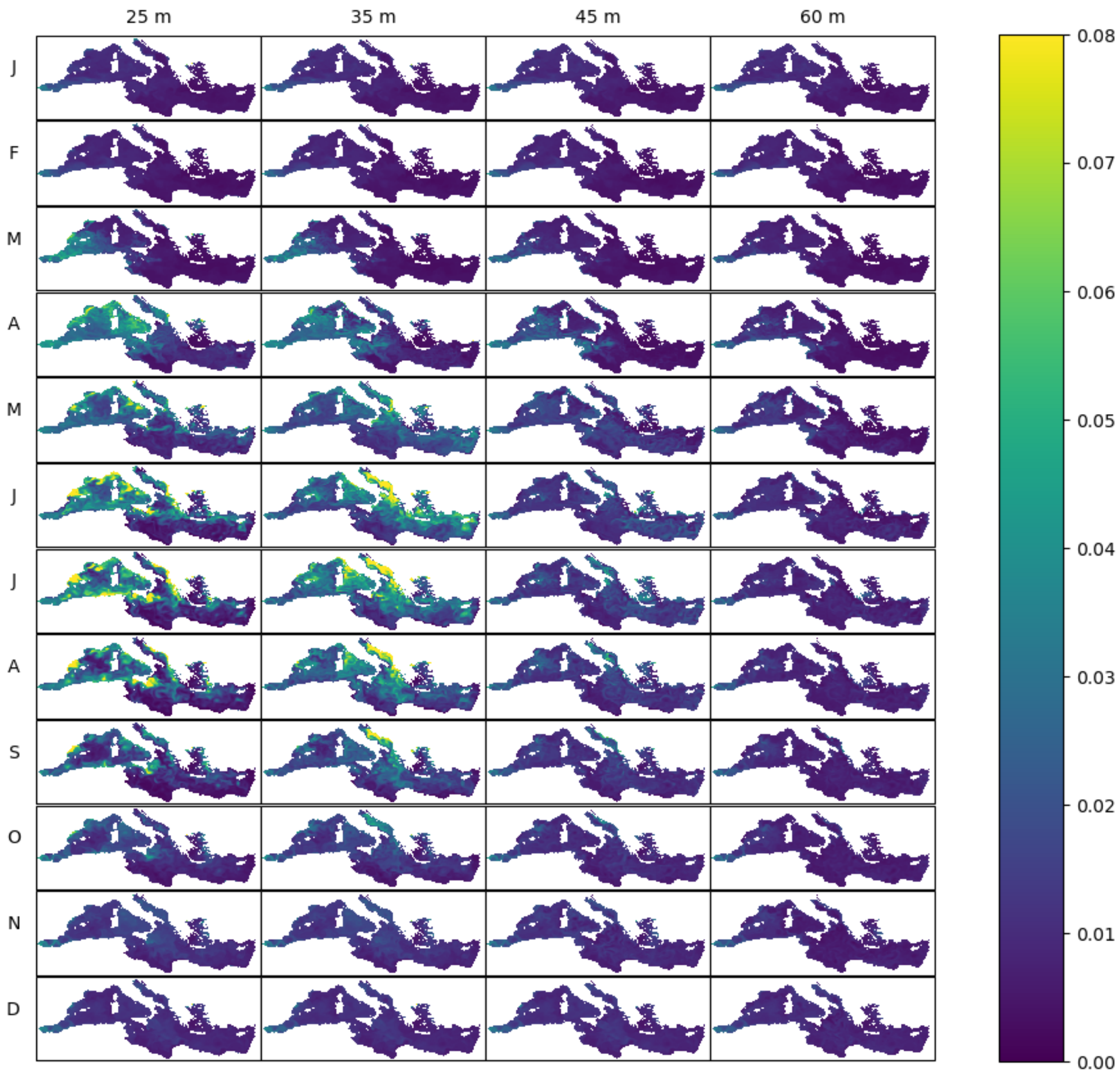

Figure S13. Spatial-temporal distribution of MMHg in large omnivorous zooplankton ($MMHg_{zoo,Z4}$).

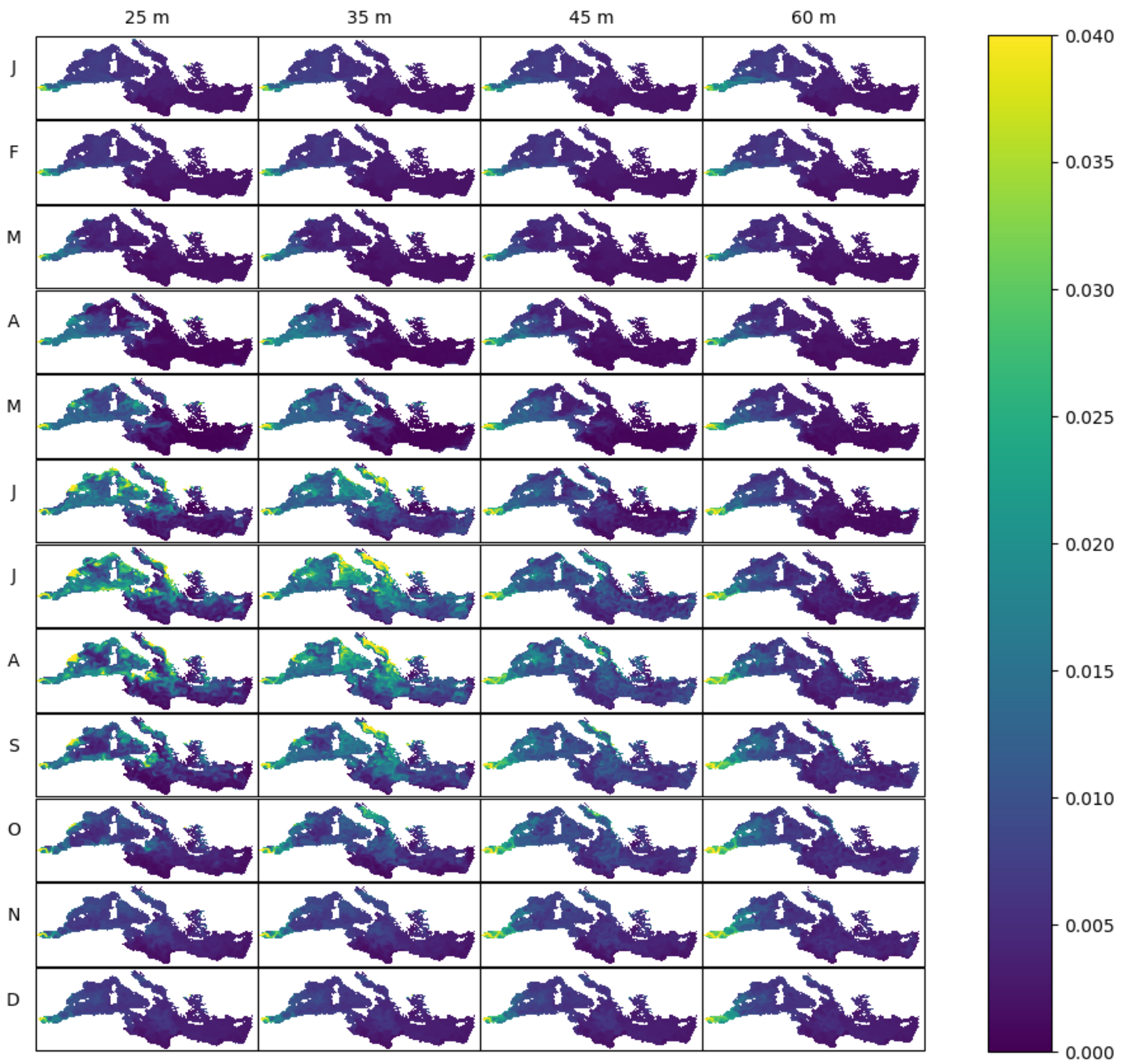

Figure S14. Spatial-temporal distribution of MMHg in large canivorous zooplankton ($MMHg_{zoo, Z3}$).

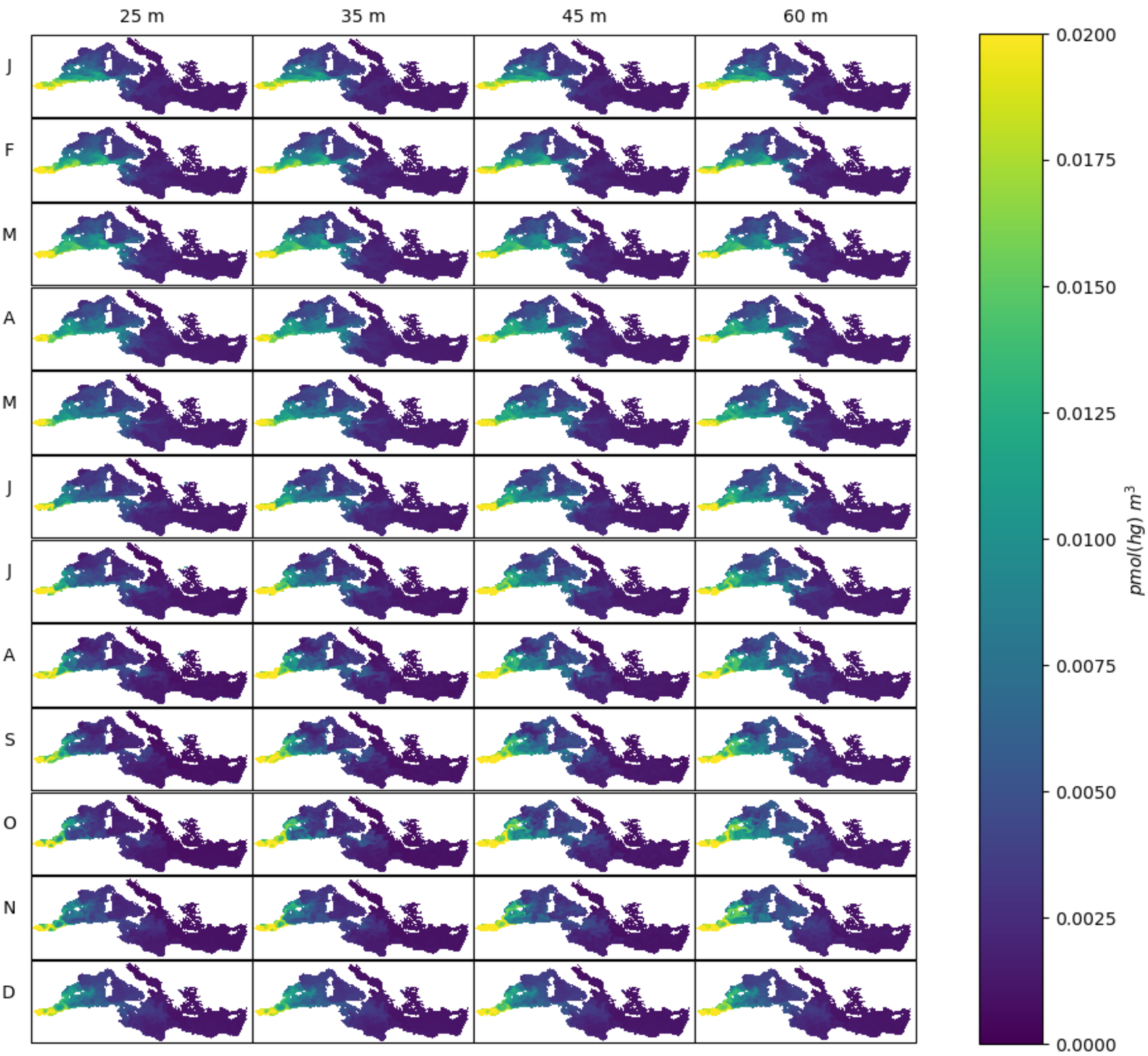

Figure S15. Spatial-temporal distribution of biomasses of heterotrophic nanoflagellates, on a carbon basis ($C_{zoo,Z6}$).

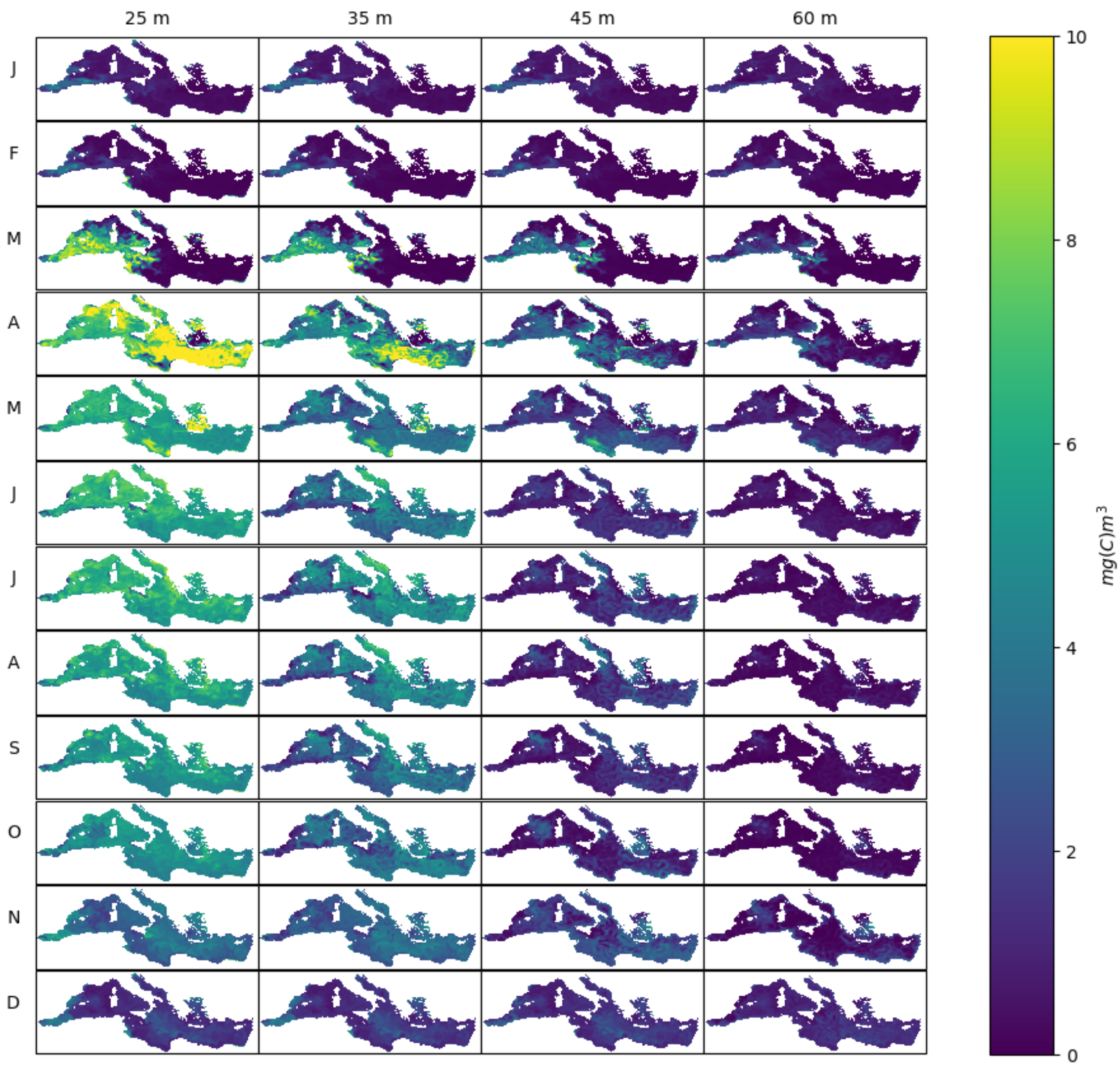

Figure S16. Spatial-temporal distribution of biomasses of carnivorous zooplankton, on a carbon basis ($C_{zoo,Z3}$).

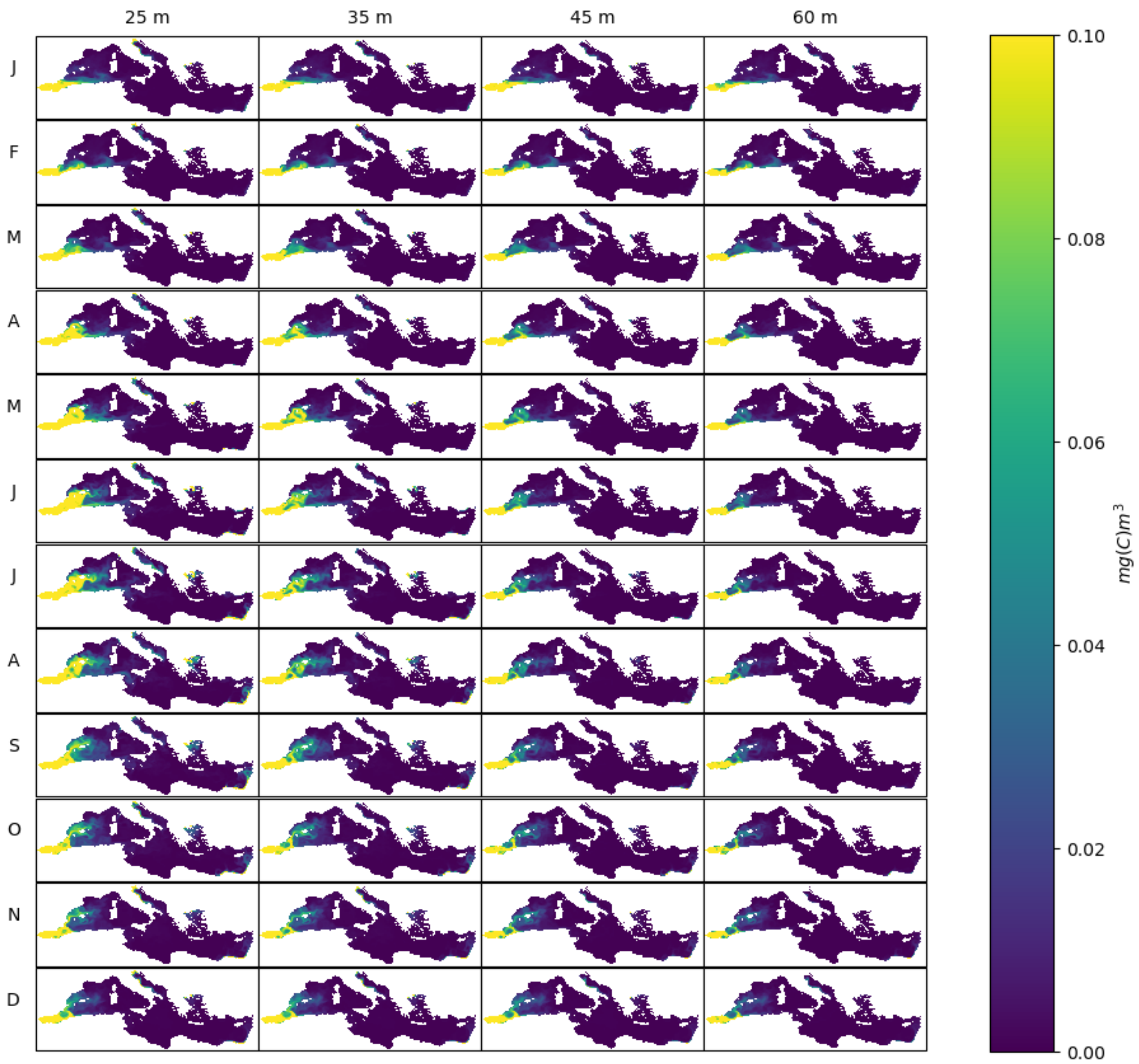

Choe, K.-Y., Gill, G. a., 2003. Distribution of particulate, colloidal, and dissolved mercury in San Francisco Bay estuary. 2. Monomethyl mercury. Limnol. Oceanogr. 48, 1547–1556. https://doi.org/10.4319/lo.2003.48.4.1547

Choe, K.-Y., Gill, G.A., Lehman, R., 2003. Distribution of particulate, colloidal, and dissolved mercury in San Francisco Bay estuary. 1. Total mercury. Limnol. Oceanogr. 48, 1535–1546. https://doi.org/10.4319/lo.2003.48.4.1547

Cossa, D., Averty, B., Pirrone, N., 2009. The origin of methylmercury in open Mediterranean waters. Limnol. Oceanogr. 54, 837–844. https://doi.org/10.4319/lo.2009.54.3.0837

Cossa, D., Durrieu de Madron, X., Schäfer, J., Guédron, S., Marusczak, N., Castelle, S., Naudin, J.J., 2018. Sources and exchanges of mercury in the waters of the Northwestern Mediterranean margin. Prog. Oceanogr. 163, 172–183. https://doi.org/10.1016/j.pocean.2017.05.002

Heimbürger, L.-E., Cossa, D., Marty, J.-C., Migon, C., Averty, B., Dufour, A., Ras, J., 2010. Methylmercury distributions in relation to the presence of nano- and picophytoplankton in an oceanic water column (Ligurian Sea, North-western Mediterranean). Geochim. Cosmochim. Acta 74, 5549–5559.

https://doi.org/10.1016/j.gca.2010.06.036

Jørgensen, S.E., Friis, M.B., Henriksen, J., Jørgensen, L.A., Mejer, H.F., 1979. Handbook of Envirnmental Data and Ecological Parameters. Pergamon Press, International Society for Ecological Modelling.

Lamborg, C.H., Hammerschmidt, C.R., Bowman, K.L., 2016. An examination of the role of particles in oceanic mercury cycling. Philos. Trans. R. Soc. A Math. Phys. Eng. Sci. 374, 20150297. https://doi.org/10.1098/rsta.2015.0297

Ward, B.A., Dutkiewicz, S., Jahn, O., Follows, M.J., 2012. A size-structured food-web model for the global ocean. Limnol. Oceanogr. 57, 1877–1891. https://doi.org/10.4319/lo.2012.57.6.1877

Zhang, Y., Jaeglé, L., Thompson, L., 2014. Natural biogeochemical cycle of mercury in a global three-dimensional ocean tracer model. Global Biogeochem. Cycles 28, 553–570. https://doi.org/10.1002/2014GB004814

Zhang, Y., Soerensen, A.L., Schartup, A.T., Sunderland, E.M., 2020. A global model for methylmercury formation and uptake at the base of marine food webs. Global Biogeochem. Cycles 1–21. https://doi.org/10.1029/2019GB006348